On the information content in linear horizontal delay gradients estimated from space geodesy observations

Gunnar Elgered[1], Tong Ning[2], Peter Forkman[1], and Rüdiger Haas[1]

[1]Department of Space, Earth and Environment, Chalmers University of Technology, Onsala Space Observatory, SE-43992 Onsala, Sweden.
[2]Lantmäteriet (The Swedish Mapping, Cadastral and Land Registration Authority), SE-80182, Gävle, Sweden

Correspondence: Gunnar Elgered (gunnar.elgered@chalmers.se)

Abstract. We assess the quality of estimated linear horizontal gradients in the atmospheric propagation delay above ground-based stations receiving signals from the Global Positioning System (GPS). Gradients are estimated from 11 years of observations from five sites in Sweden. Comparing these gradients with the corresponding ones from the European Centre for Medium-Range Weather Forecasts (ECMWF) analyses show that GPS gradients confirm known seasonal effects both in the

5   hydrostatic and the wet components. The two GPS sites equipped with microwave absorbing material below the antenna in general show higher correlation coefficients with the ECMWF gradients compared to the other three sites. We also estimated gradients using GPS data from two collocated antenna installations at the Onsala Space Observatory. Correlation coefficients for the east and the north wet gradients from GPS can for specific months reach up to 0.8 when compared to simultaneously estimated wet gradients from microwave radiometry. Based on the four years of results we note a strong seasonal dependence,

10   from 0.3 during months with smaller gradients to 0.8 during months with larger gradients, typically during the warmer, and more humid, part of the year. Finally, a case study using a 15 days long continuous Very Long Baseline Interferometry (VLBI) campaign was carried out. The comparison of the gradients estimated from VLBI and GPS data indicates that a homogeneous sampling of the sky is a critical parameter.

1   Introduction

15   Space geodetic techniques, where the fundamental observable is a radio signal's time of arrival at a site on the surface of the Earth, are affected by variations in the propagation velocity in the atmosphere. Because time measurements avoid problems related to accurate calibration, which are common for systems measuring different types of emissions, it is a common view that Global Navigation Satellite Systems (GNSS) have a long term stability and are well suited for climate monitoring, e.g. in terms of the atmospheric water vapour content. Estimates of the total propagation delay above a GNSS site can be used

20   to determine the integrated amount of water vapour. It is also common practice to estimate two-dimensional horizontal linear gradients for each site in the GNSS data processing, because it improves the reproducibility of estimated geodetic parameters, see e.g. (Bar-Sever et al., 1998).

We address the question of the quality of the estimated gradients primarily from GPS data from Swedish GNSS sites by comparing these gradients to independent measurements. An important site is the fundamental geodetic station at the Onsala
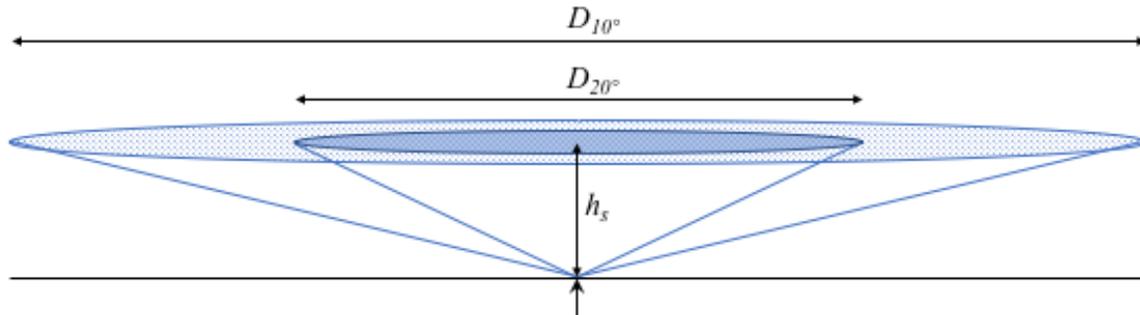
Figure 1. The atmospheric volume determining the estimated atmospheric parameters is a cone originating at the upward pointing arrow. The scale heights, h_s of the hydrostatic refractivity and the wet refractivity are approximately 8 km and 2 km, respectively. For the hydrostatic refractivity the diameter of the cone at the scale height is 91 km ($D_{10°}$) and 44 km ($D_{20°}$) for the elevation cutoff angles equal to $10°$ and $20°$, respectively. The corresponding diameters for the cones representing the wet refractivity are 23 km and 11 km, respectively. Note that the horizontal and vertical scales are different.

Space Observatory where a geodetic Very Long Baseline Interferometry (VLBI) telescope and a water vapour radiometer (WVR) are installed collocated to GNSS receiver stations. The overall goal is to thereby assess the usefulness of GPS-derived gradients in atmospheric and climate research. Previous studies have been carried out using GPS/GNSS data from Onsala. Comparing the horizontal gradients derived from VLBI), GPS, and a WVR, Gradinarsky et al. (2000) found that using different

5   constraints for the variability of the horizontal gradient in the VLBI and GPS data analysis did not have a significant impact on the agreement with the WVR estimates. A more recent study by Li et al. (2015) reported on the improvement obtained by using multi-GNSS constellations instead of GPS only.

In Section 2 we give a short background on the cause of horizontal gradients that are sensed by the space geodetic techniques. In Section 3 instruments, techniques, and their data are described. The results are presented in two sections. First, in Section 4,

10   we use 11 years of data to study the gradients from five Swedish GNSS sites and assess their quality by comparing them to gradients originating from the European Centre for Medium-Range Weather Forecasts (ECMWF) analyses. In Section 5, we use data from two collocated GNSS sites and one WVR to assess the accuracy of the gradients during a four year period. Within this period we also carry out a comparison to gradients estimated from a 15 day long VLBI campaign. Finally, in Section 6 we present our conclusions and discuss possible future studies of gradients.

15   **2   Cause of horizontal gradients**

The refractivity in the atmosphere is determined mainly by the total pressure, the temperature and the partial pressure of water vapour. The atmospheric volume sensed by a GNSS instrument is illustrated in Figure 1.

Hydrostatic gradients are usually dominated by pressure gradients and exist mainly over global and regional scales (e.g. mesoscale weather systems). For example the north gradient has a clear dependence of pressure and latitude when averaged

20   over long time scales. This has been shown by Meindl et al. (2004). For the area of interest in this study we specifically mention

the Icelandic low pressure system that typically evolves in the winter and disappears in the summer, e.g. (Hewson and Longley, 1944).

Temperature and especially water vapour can show relatively much stronger horizontal gradients over small (kilometre) scales. The temporal variability is typically also much higher than that of the hydrostatic gradients, see e.g. Li et al. (2015).

5 Hence, the large local gradients over a site are mainly caused by the variability in water vapour and the wet refractivity. Gradients can be significant during a passage of a weather front, especially for distinct cold fronts. Other specific weather phenomena that can cause horizontal variability are sea breeze (Munn, 1966), cloud rolls (Brown, 1970) and convection processes in general. We note that none of the known processes is expected to be strictly linear, but the strength in the geometry and the GNSS data quality have so far not motivated attempts to determine additional atmospheric parameters of higher order.

10 ## 3 Instrumentation and data

We compare horizontal gradients estimated from GPS observations acquired at five sites and six antenna/receiver installations: Kiruna (KIR0), Mårtsbo (MAR6), Onsala (ONSA and ONS1), Borås (SPT0), and Visby (VIS0). These sites are also part of the EUREF network (Bruyninx et al., 2012). Their geographic locations are shown in Figure 2 and the used datasets are summarised in Table 1.

Table 1. Summary of used datasets.

Dataset[1]	Resolution	Time period	ONS1	ONSA	SPT0	VIS0	MAR6	KIR0
GPS (10°)	5 min	2006–2016	–	√	√	√	√	√
GPS (10°)	5 min	2013–2016	√	√	–	–	–	–
GPS (20°)	5 min	2013–2016	√	√	–	–	–	–
WVR	15 min	2013–2016	√	√	–	–	–	–
VLBI	6 h	6–20 May 2014	√	√	–	–	–	–
ECMWF[2]	6 h	2006–2016	√	√	√	√	√	√

[1] The GPS datasets have been processed with elevation cutoff angles equal to 10° or 20°

[2] (Boehm and Schuh, 2007)

15 ### 3.1 GPS

We used 11 years of GPS data (2006–2016) from the five Swedish GNSS sites mentioned above. Linear horizontal gradients in the east and the north directions were estimated with a temporal resolution of 5 min. Two GNSS sites are operating continuously at the Onsala Space Observatory, on the west coast of Sweden. The primary site, ONSA, was established already in 1987 and the other site, ONS1, was taken into operation in 2011. The six antenna sites are shown in Figure 3. The antennas of ONSA
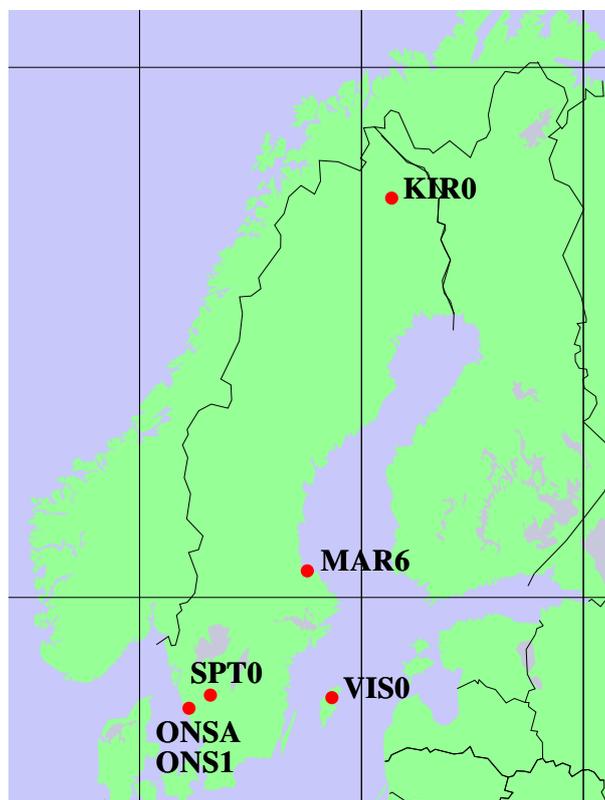
Figure 2. The six GPS sites used in the study. ONSA and ONS1 are collocated together with the VLBI telescope and the WVR at the Onsala Space Observatory.

and ONS1 are located within 100 m from each other and should observe almost identical atmospheric gradients. For the time period 2013–2016 we compare gradients from these two sites with simultaneously estimated gradients using data from a WVR.

The analysis of the GPS data follows the same lines as described by Ning et al. (2013) and is summarised in Table 2. Based on the five-minute gradients we calculated mean values over 15 min, 1 h, 6 h, 1 day, and 1 month.

5 An example of the sky coverage of the GPS observations is shown in Figure 4 for the Onsala site. At this latitude there is a significant part of the sky that is never sampled, just north of the zenith direction. It is reasonable to assume that this will have a negative impact on the estimated gradients, and especially in the north direction.

3.2 Microwave radiometer

The microwave radiometer is designed in order to provide independent estimates of the wet propagation delays for space

10 geodetic applications. It measures the emission from the sky, on and off the water vapour line at 22.2 GHz. Its specifications are summarised in Table 3.

During the time period 2013–2016 the WVR was observing in a sky mapping mode as is illustrated in Figure 6. A disadvantage of a WVR is that the algorithm for calculation of the wet propagation delay breaks down for data acquired during rain or

Figure 3. The six antenna installations used to acquire the GPS data.

Table 2. Processing of GPS data.

Parameter	Description / Value
Processing software	GIPSY v6.2 (Webb and Zumberge, 1993)
Strategy	Precise Point Positioning (Zumberge et al., 1997)
Mapping function	Vienna 1 2006 (VMF1) (Boehm et al., 2006)
Elevation cutoff angle	$10°$ or $20°$
Zenith delay	Estimated every 5 min, constraint 10 mm/$\sqrt{h}$
Linear horizontal gradient	Estimated every 5 min, constraint 0.3 mm/$\sqrt{h}$
Ocean tide model	FES2004 (Lyard et al. , 2006)
Antenna phase centre	igs_1740.atx (Schmid et al., 2007)
Ambiguity resolution	Yes (Bertiger et al., 2010)
Ionosphere model	2nd order (IGRF)[1] (Matteo and Morton, 2011)

[1] International Geomagnetic Reference Field
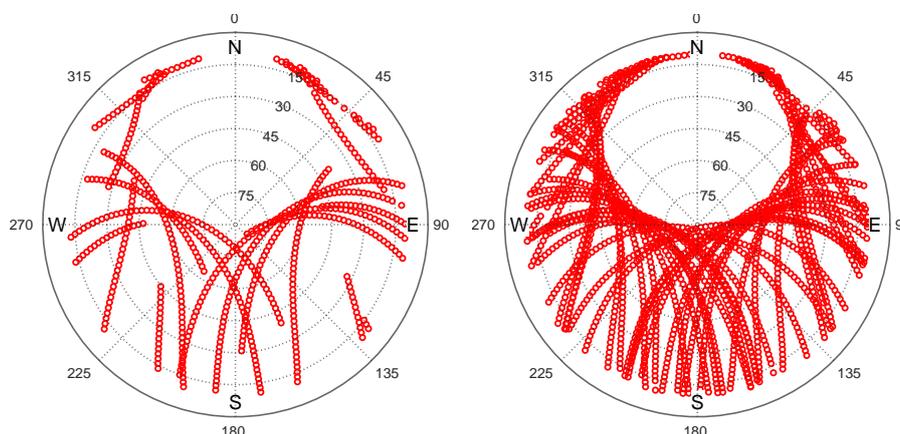
Figure 4. Sky plot of GPS observations from 6 to 12 UT (left) and from 0 to 24 UT (right) on May 12, 2014.

when large liquid drops are present in the sensed atmosphere. Therefore, data taken during rain, or when the estimated amount of liquid water is >0.7 mm, are discarded from the analysis. In addition there are also time periods when the WVR hardware has failed. The analysed data are shown in Figure 7 as the number of individual observations per day.

The WVR gradients are estimated based on all observations carried out during a 15 min period using the method of least squares. We used the so called four-parameter model, fitting a zenith wet delay (ZWD), a ZWD rate, and an east and a north linear horizontal gradient to the data (Davis et al., 1993). This means that the estimated gradients are independent of the

Figure 5. The water vapour radiometer (WVR) Konrad at the Onsala Space Observatory.

Table 3. Specifications for the Konrad WVR.

Parameter	Value
Frequencies	20.6 GHz and 31.6 GHz
Antenna type (one for each channel)	Conical horn with lens
Antenna beam FWHM[1], E-plane, ch.1 / ch.2	2.9°/ 2.0°
Antenna beam FWHM[1], H-plane, ch.1 / ch.2	3.4°/ 2.3°
Reference temperatures (both channels)	313 and 373 K
System noise temperatures, channel 1 / 2	450 / 550 K
RF bandwidth (double sideband)	320 MHz (both channels)
Absolute accuracy (weather dependent due to the quality of tip curves)	1–3 K
Repeatability	0.1 K

[1] FWHM = Full Width Half Maximum

adjacent estimates, which is different from the gradients estimated from the space geodetic techniques, where constraints with time are applied.
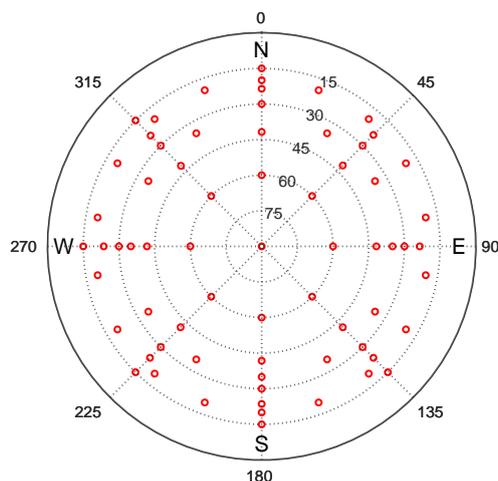
Figure 6. A measurement cycle with the WVR begins with two azimuth scans. Starting in the north, first at an elevation angle of $20°$ clockwise to the north, and then counterclockwise at an elevation angle of $35°$. Thereafter four tip curves are made over the zenith direction (implying that four observations are made in the zenith direction during each cycle): from the north to the south, from the southwest to the northeast, from the east to the west, and from the northwest to the southeast. The cycle is about 8 min long and is repeated continuously, implying that almost two complete cycles are executed during the time of the highest temporal resolution used, i.e. 15 min.
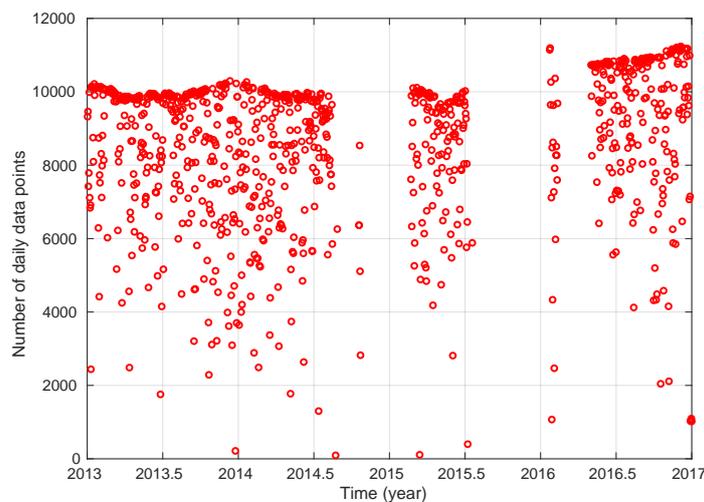
Figure 7. Number of data points per day observed by the WVR. During days without data loss, e.g. due to rain, each estimated gradient is based on approximately 100 observations in the directions illustrated in Figure 6. During the last year the measurement cycle was optimised by reducing some of the time delays inserted between samples.

3.3 ECMWF data

The Technical University of Vienna provides horizontal hydrostatic and wet gradients based on ECMWF data for many space geodetic sites globally. Figure 2 depicts the five sites used here. Details are given by Boehm and Schuh (2007), so we just mention the characteristics that are most relevant for our comparisons. Of importance to us is the temporal resolution of 6 h,

5 which implies that the short term variability in the water vapour will be averaged out. We anticipate, however, that these data are useful to separate the hydrostatic delay gradients from the total delay gradients estimated from the GNSS data. The data are available during certain time periods from the mid of 2005 and are more continuous from 2006. We decided to use the data from 2006 to 2016, resulting in a time series of 11 years.

3.4 Very long baseline interferometry data

10 We have used the VLBI data from the CONT14 campaign coordinated by the International VLBI Service (Nothnagel et al., 2017). The campaign was observed during May 6–20, 2014. The VLBI data were analysed with the calc/solve VLBI data analysis software (Ma et al., 1990). Station positions, ZWD, atmospheric horizontal gradients, relative clock parameters w.r.t. a reference station, as well as earth rotation parameters were estimated. The relative clock parameters were estimated as piece-wise linear offsets every hour, with a constraint of 5.0^{-14} s/s between clock rate segments. The ZWD and atmospheric gradients

15 were estimated as piece-wise linear offsets with a temporal resolution of 30 min and 6 h, respectively. Constraints of 15 mm/h between ZWD rate segments, 0.5 mm for gradient offsets and 2 mm/day for gradient rates were applied. The NMF (Niell, 1996) mapping functions were used in the analysis, together with meteorological information recorded at the VLBI stations.

Figure 8 depicts the sampling of the sky for a 6 h period which is the highest temporal resolution of the gradient estimates from VLBI as well as all observations scheduled for a 24 h experiment. This schedule was repeated every day with only minor

20 modifications.
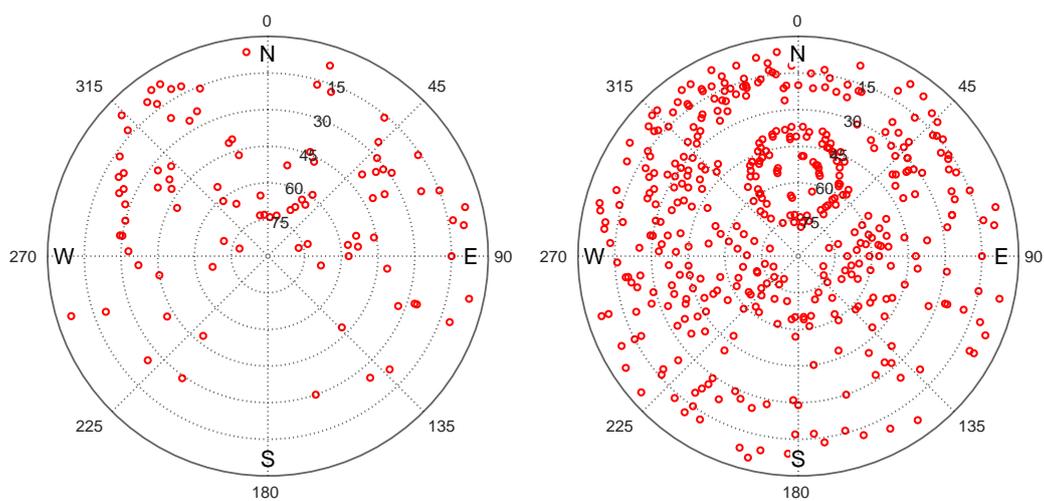
Figure 8. The directions of the VLBI observations for the time period from 6 to 12 UT (left) and from 0 to 24 UT (right), both on May 12, 2014.

4 Comparison of gradients from GPS and ECMWF data

4.1 Seasonal variations of horizontal gradients

We start by investigating the characteristics of the gradients over the year. In Figure 9 we present the monthly mean gradients for the time period 2006–2016 estimated from ECMWF data and GPS data from the Onsala (ONSA) site.

5   We can clearly see negative north gradient in the winter both in the GPS and the ECMWF results. When the ECMWF gradients are separated into the hydrostatic and the wet components this variation appears in the hydrostatic component. We interpret this effect as the influence of the Icelandic low pressure system (Hewson and Longley, 1944). Another feature is seen in the ECMWF wet gradients. They are larger in the summer when the wet refractivity is higher, and, at least according to the ECMWF data, there is a tendency to a positive east gradient in the summer. The ONSA GPS site is located a few hundred

10   metres from the coastline, suggesting that the air on the average is more humid over land compared to over the sea in the ECMWF model. The issue of wet gradients is studied further using a higher temporal resolution and comparisons with the WVR data in Section 5.1.

    The results for the other four sites (KIR0, MAR6, SPT0, and VIS0) show identical systematic features except KIR0, which is at a higher latitude and is less humid. At KIR0 the average monthly wet gradients are insignificant except during the summer

15   months. Furthermore, the influence of the Icelandic low pressure in the winter is not as large as it is at the other four sites.
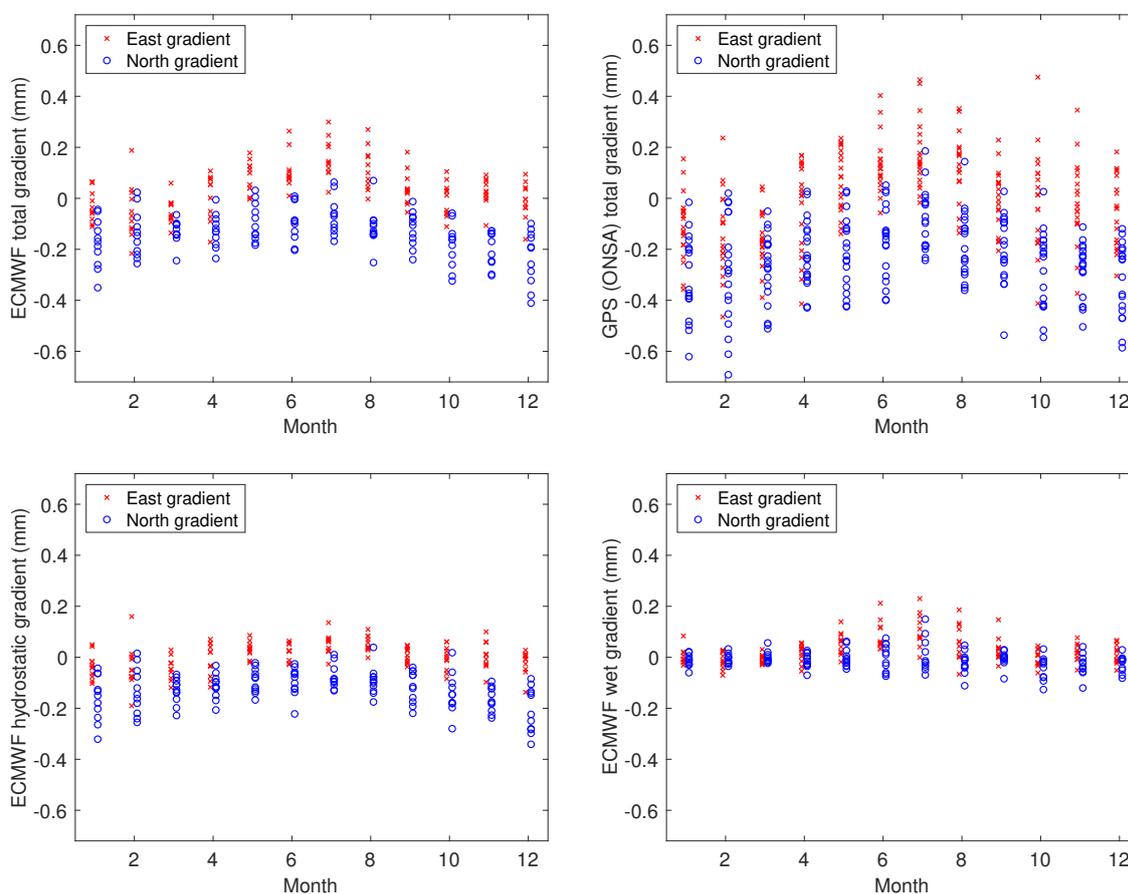
Figure 9. Monthly means of estimated gradients at the Onsala site for the period 2006–2016. The top graphs show the total gradients from ECMWF (left) and GPS (right). The graphs at the bottom show the ECMWF gradients when separated into the hydrostatic (left) and the wet gradient (right).

Table 4. Correlation coefficients for the total east and north linear horizontal gradients estimated from GPS data and compared to ECMWF data.

Site	Hourly		Daily		Monthly	
	East	North	East	North	East	North
Kiruna (KIR0)	0.55	0.53	0.76	0.75	0.77	0.82
Mårtsbo (MAR6)	0.58	0.51	0.75	0.72	0.83	0.80
Onsala (ONSA)	0.60	0.60	0.75	0.78	0.90	0.90
Borås (SPT0)	0.58	0.58	0.74	0.74	0.88	0.85
Visby (VIS0)	0.55	0.56	0.71	0.75	0.84	0.81

4.2 Comparing GPS and ECMWF gradients over different time scales at the five sites

We assess the data quality, in terms of correlation coefficients, between the total GPS and ECMWF gradients estimated at the 5 GPS sites using data from 2006 to 2016. These are shown in Table 4.

The correlations seen in all cases confirm that an atmospheric signal in terms of linear gradients is detected by the GPS observations. We note that the correlation coefficients increase for longer averaging time periods. Our interpretation is that by long term averaging we compare a larger fraction of the gradient that is caused by large scale temperature and pressure gradients, which is better modelled by the ECMWF data. Unfortunately, the temporal resolution of 6 h in the ECMWF data is not sufficient to resolve neither rapid changes in the pressure related to moving weather systems nor many of the short lived small-scale gradients associated with the variability in the water vapour.

Another result worth noting is that the two sites with the highest correlation coefficients, and especially for the monthly averages, are ONSA and SPT0. These two sites are the only ones that are equipped with microwave absorbing material below the antenna. This could reduce the impact from unwanted multipath effects. The phenomenon calls for further studies.

Assuming that the ECMWF hydrostatic gradients, linearly interpolated between the 6 h values, are reasonably accurate we have the possibility to subtract this hydrostatic gradient from the estimated total GPS gradient in order to compare the wet gradients at these five sites. In Table 5 we present the mean values and the standard deviation of these for the three different temporal resolutions. We note that when the wet gradients are averaged over one hour and one day, the standard deviations (SD) obtained for the KIR0 site are significantly smaller. This is likely a consequence of the lower humidity at the site. For monthly averages, however, all sites have comparable SD, indicating that at this low level other effects become important.

Given that horizontal gradients in general are small and that the larger values typically occur for a short time we expect that any long-term trends would be very small and therefore also difficult to detect. An estimated gradient has a direction and from a time series we estimate trends for the east and the north gradients. Combining these two trends offers the possibility to also search for trends in the total amplitude value of the gradient at the site. A positive trend in the amplitude will occur if there

Table 5. Mean values and standard deviations (SD) over the 11 years of estimated horizontal wet gradients from GPS data for different temporal resolutions.

Site	ZWD[1]		Horizontal gradient								
			Mean[2]		Hourly SD		Daily SD		Monthly SD	
	Mean	SD	East	North	East	North	East	North	East	North
	(mm)	(mm)	(mm)	(mm)	(mm)	(mm)	(mm)	(mm)	(mm)	(mm)
Kiruna (KIR0)	61	36	−0.20	−0.02	0.41	0.43	0.23	0.24	0.09	0.09
Mårtsbo (MAR6)	88	46	−0.22	−0.02	0.50	0.53	0.30	0.28	0.11	0.11
Onsala (ONSA)	92	47	0.01	−0.08	0.54	0.50	0.32	0.30	0.13	0.10
Borås (SPT0)	87	45	−0.06	−0.12	0.50	0.49	0.30	0.30	0.12	0.12
Visby (VIS0)	88	47	−0.06	−0.10	0.55	0.51	0.32	0.29	0.12	0.09

[1] The Zenith Wet Delay (ZWD) is included to illustrate the amount of water vapour in the atmosphere above the site.

[2] The mean gradient values are based on the 1 h gradient averages.

is an increase in the variability at the site, which can happen even if there are no trend, neither in the east, nor in the north gradients. For these five sites we have estimated linear gradients in the east and the north direction as well as for the gradient amplitudes over the 11 years. The trends are indeed very small. Typically they are all well below 0.01 mm/year. The highest value is −0.02 mm/year for the wet gradient in the north direction at the SPT0 site. If this trend originates from the atmosphere

5 it is a local effect because it is 6 times as large as the wet north gradient trend at the nearby ONSA site. On the other hand we cannot rule out that it is an effect due to a not perfectly stable hardware at the site, although it is far from as dramatic as the problems reported by Douša et al. (2017).

5 Gradients at the Onsala site

5.1 Wet gradients

For the Onsala site we have total gradients from the two GPS sites, hydrostatic and wet gradients from ECMWF, and wet gradients from the WVR. First we compare the total gradients in the east and the north direction from the GPS data. A comparison is shown in Figure 10. We expect that the two GPS sites share several error sources and therefore there is a significant common mode suppression of errors, meaning that the rather high correlation may be slightly overoptimistic.
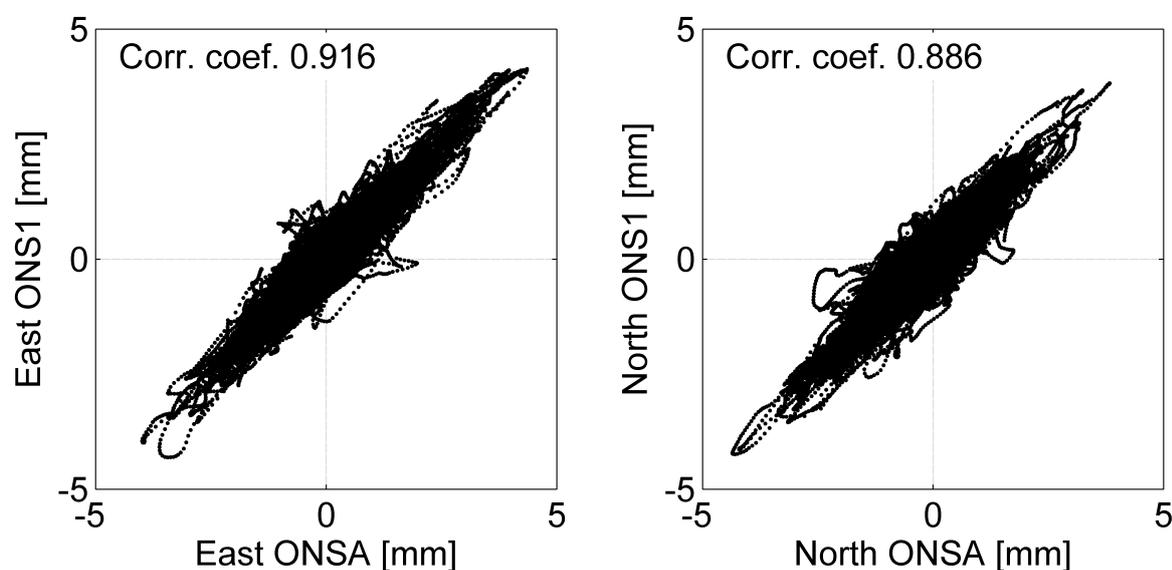
Figure 10. Correlations between estimated total gradients from the GPS sites ONSA and ONS1 using all data from the period 2013–2016.

In order to compare the wet gradients, the hydrostatic gradients from ECMWF, linearly interpolated to match the time epochs of the GPS gradients, are subtracted from the estimated total GPS gradients. Thereafter we form 15 min averages for the east and the north wet gradients from GPS and compare to the corresponding WVR results. Correlation plots are shown in Figure 11.

As expected, the correlations between the estimated gradients from the two GPS sites are significantly higher compared to when the GPS gradients are correlated with the gradients from the WVR. It is also not surprising that the correlation between wet gradients from ONSA and ONS1 are slightly lower compared to the correlation between the total gradients (Figure 10). When subtracting the hydrostatic gradients, the dynamic range is reduced, which affects the correlation coefficients. Furthermore, the sampling on the sky agrees also much better between the two GPS sites, assuming that in general the directions of the observations are towards the same satellites, whereas the WVR's observations are evenly spread over the sky.

We also note that the correlations are in general higher for the east gradient, possibly because of the poorer sampling on the sky north of the zenith direction due to the geometry of the GPS satellite constellation (see Figure 4). Another issue related
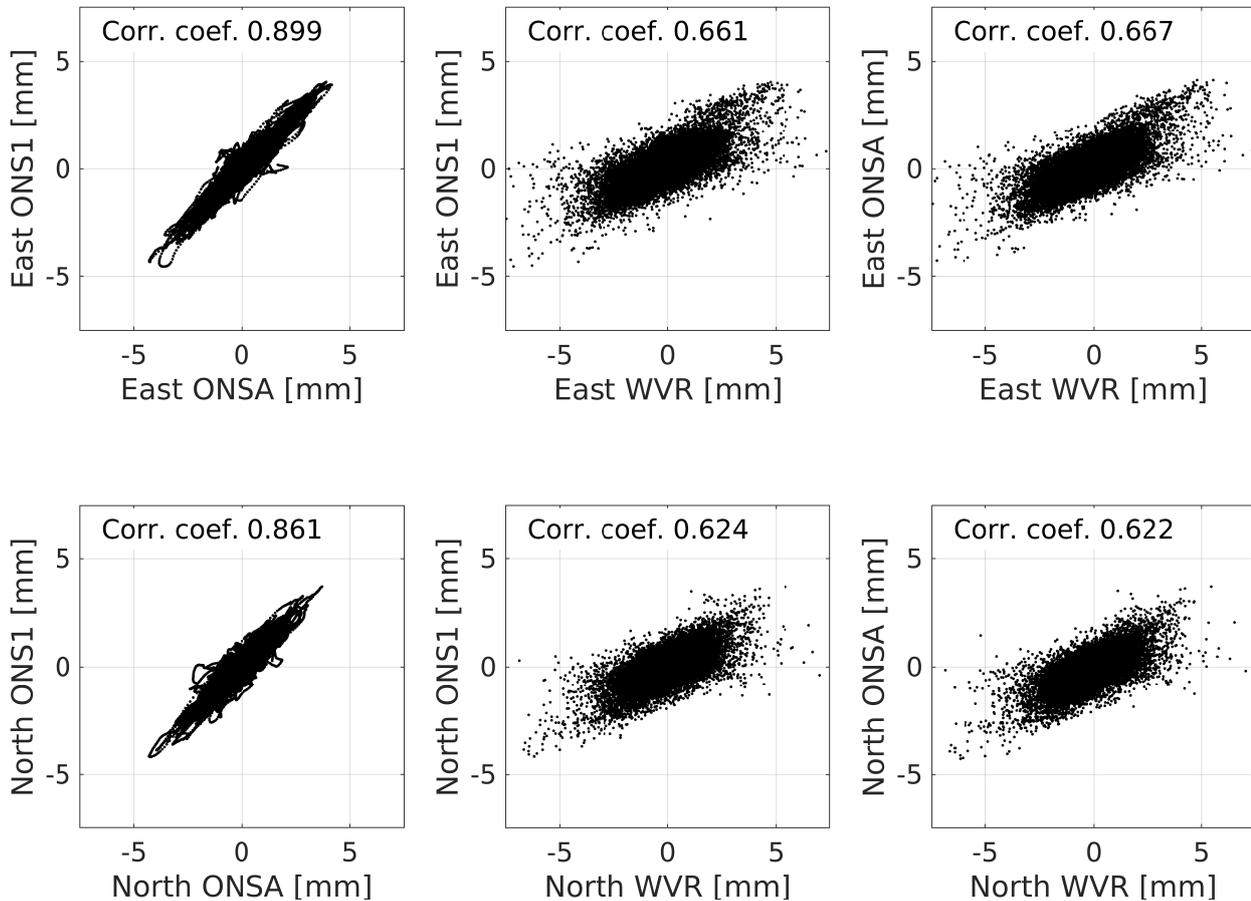
Figure 11. Correlations between estimated wet gradients from the WVR and the wet gradients from GPS data using all data from the period 2013–2016.

to the sky coverage of the observations is that the WVR has an elevation cutoff angle of 20 degrees in order to avoid ground-noise pickup. Therefore, we also processed the GPS data with an elevation cutoff angle equal to 20 degrees, expecting that a better agreement between the spatial sampling of the WVR and GPS would result in higher correlation coefficients. All the correlation coefficients in Figure 11 were, however, reduced at the order of 10 %. One interpretation of this result is that for

5   the temporal resolution of 15 min the low elevation observations are important in order to distinguish the gradient parameters relative to other estimated parameters in the GPS analysis. Therefore we will not present these results in any more detail.

We investigated if an average of the estimated wet gradients from ONSA and ONS1 will improve the agreement with the WVR. The result is shown in Figure 12. Comparing Figure 12 with Figure 11 we see an overall small improvement. For the east gradient the individual correlations coefficients were improved from 0.667 (ONSA) and 0.661 (ONS1) to 0.687. The

10 corresponding values for the north gradient were from 0.622 (ONSA) and 0.624 (ONS1) to 0.649. Our interpretation is that by averaging the GPS gradients from ONSA and ONS1 the stochastic noise is reduced. We identify that the lack of a perfect

correlation is due to at least two remaining reasons. One is the systematic effect caused by the different sampling on the sky. The use of a multi-GNSS constellation has been shown to improve the agreement (Li et al., 2015). The other reason is the much higher variability in the time series from the WVR because no temporal constraints are used when estimating these gradients.
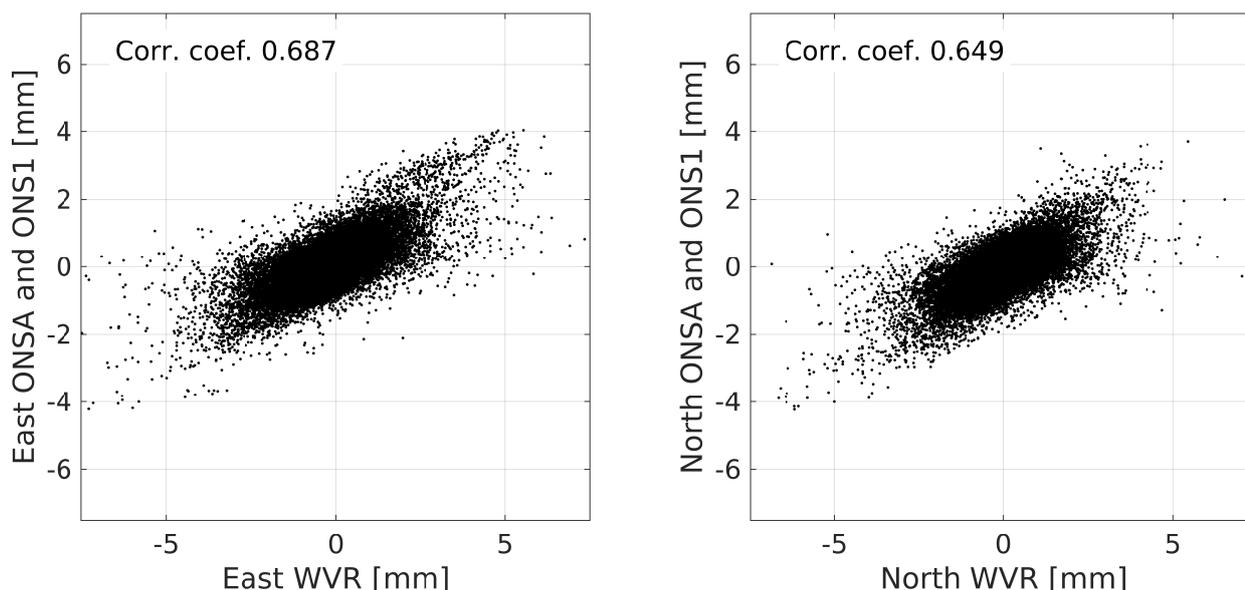
Figure 12. Correlations between the mean values of ONSA and ONS1 wet gradients and the WVR gradients using all data from the period 2013–2016.

Correlation plots are shown in Figure 13 for each month of the four years. A clear seasonal dependence is seen, because the
5 variability in the wet refractivity is larger during the warmer time periods, resulting in larger gradients and a larger dynamic range. In a study by Lu et al. (2015) a correlation coefficient of 0.52 was reported for the months March–May, 2014, between GPS and WVR gradients. Here we show that the variability from month to month is large and therefore the choice of the time period for gradient comparison studies is a critical issue.

Comparing the results obtained for ONSA with those from ONS1 they are almost identical (in both Figures 11 and 13)
10 meaning that in this case there is no obvious improvement from the absorbing material below the antenna on ONSA. This is different to the previous finding where ONSA and SPT0, with microwave absorbing material, showed a better agreement with ECMWF gradients compared to the KIR0, MAR6, and VIS0 sites. Our assumption is that the lack of a concrete pillar with a metal mounting plate just below the antenna on ONS1 eliminates the need for an absorber (see Figure 3).
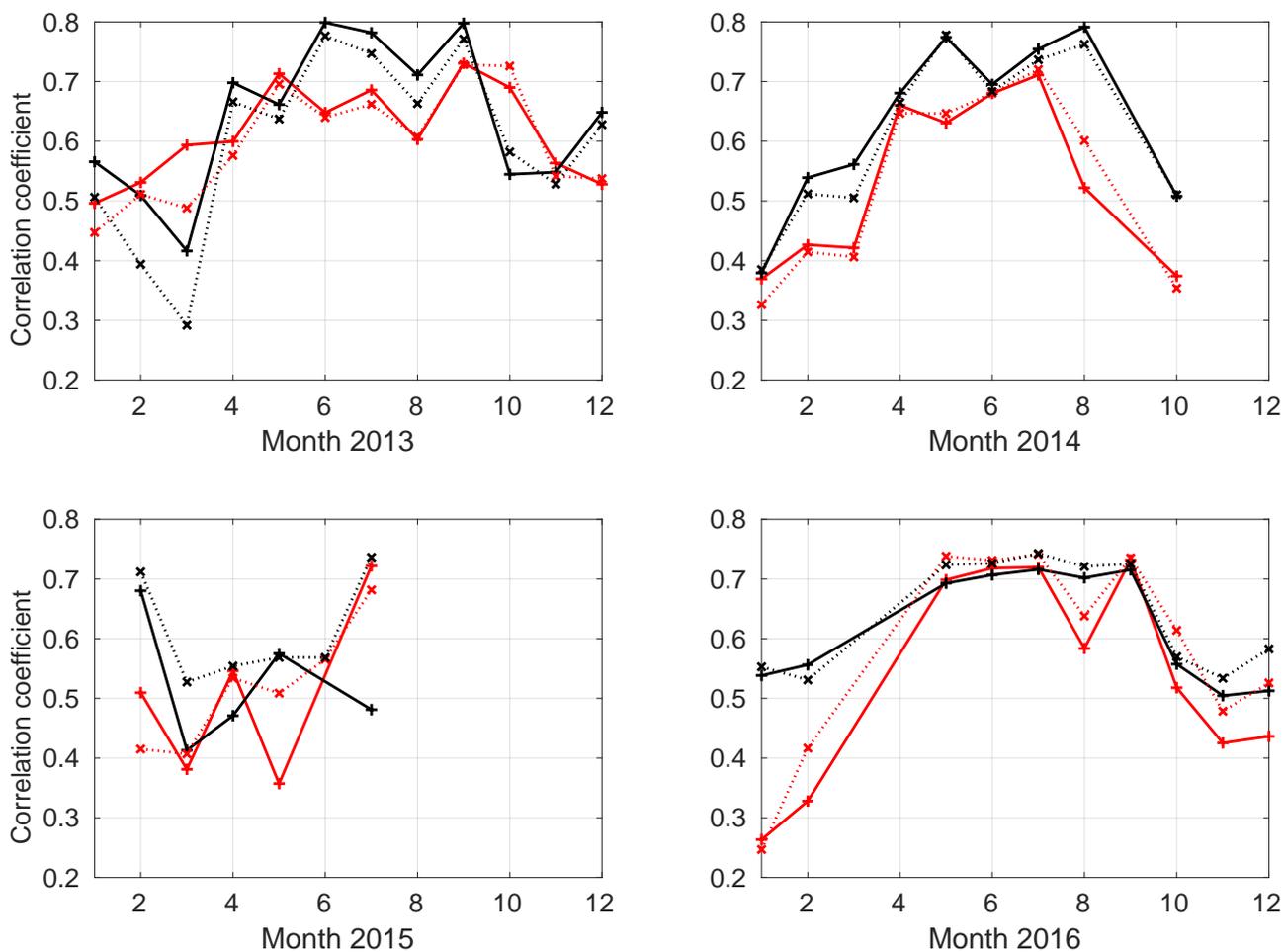
Figure 13. Correlations between estimated wet gradients averaged over 15 min from the WVR data and the different GPS data from ONSA (solid lines) and ONS1 (dotted lines) when the hydrostatic gradients have been removed from the total GPS gradients for each month of the four years. The north gradients are presented with red lines and the east gradients as black lines.

5.2 Gradients during the CONT14 VLBI campaign

The total gradients from the two space geodetic techniques GPS and VLBI were compared using the data from the CONT14 campaign. Observations from several earlier CONT campaigns have been analysed in terms of gradients with different results depending on the site and the time of the campaign (Teke et al., 2013). Here we focus on GPS and VLBI data from the Onsala site. The estimated time series are shown in Figure 14. Correlation plots for the east and the north gradients compared to the two GPS sites, ONSA and ONS1, are presented in Figure 15. We note that the agreement in general is better for the east component compared to the north. There is a specific example seen during day 132 (May12) where a large north gradient is not detected in the VLBI data. The independent wet gradients obtained from the WVR (not shown) confirm that this gradient was originating from the atmosphere. The left plot in Figure 8 may explain why the north gradient has a larger uncertainty at this specific time. We attribute the slightly lower correlation coefficients obtained between GPS-VLBI compared to GPS-WVR for the month of May 2014 in Figure 13 to the sparse sequential sampling of the sky by the VLBI observations. The future use of the twin telescopes at the site is likely to improve this situation which in turn should improve the accuracy of the estimated atmospheric parameters in VLBI experiments.
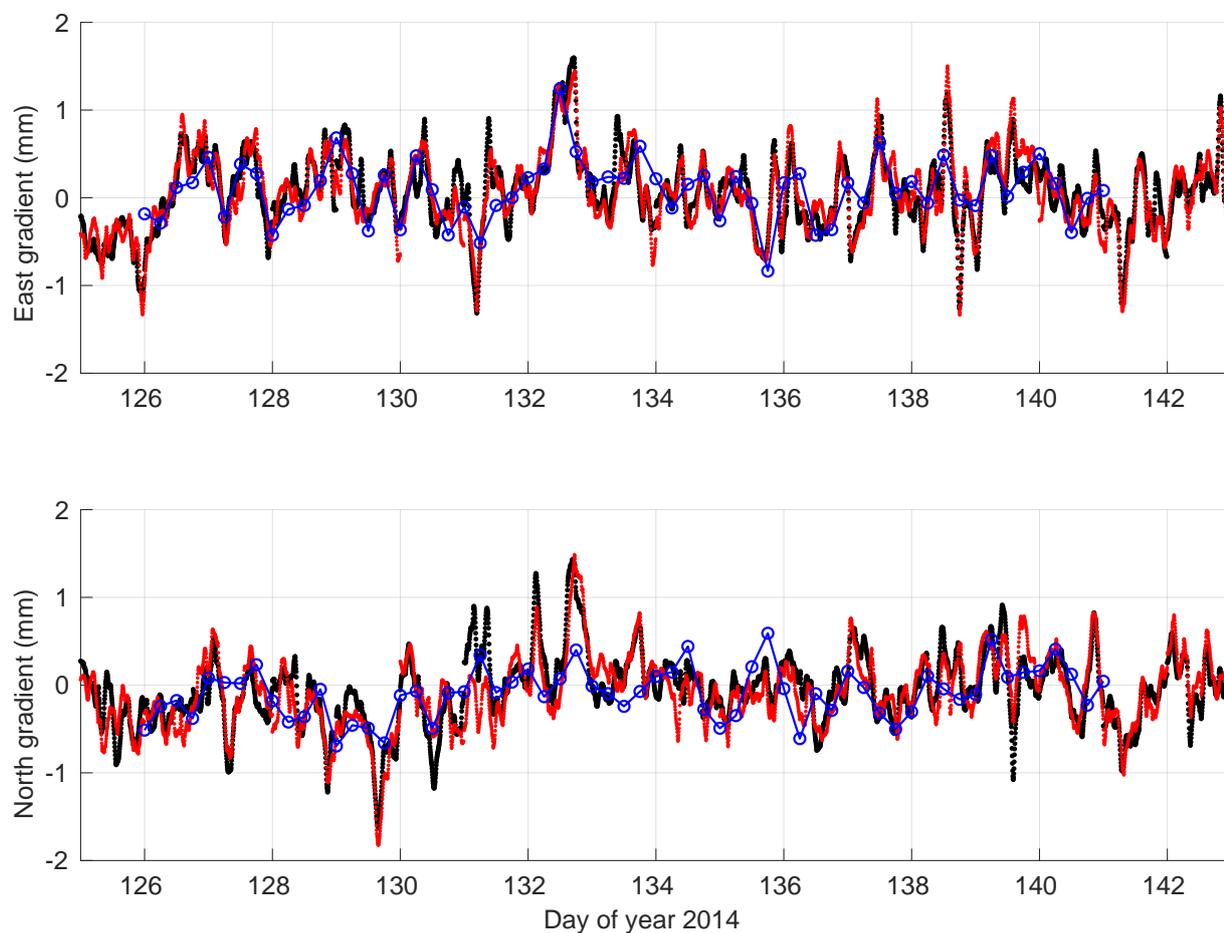
Figure 14. Time series of estimated total east (top) and north (bottom) gradients from VLBI and GPS data. The temporal resolution is 6 h for the VLBI gradients (blue circles connect with a solid line), 5 min for the GPS gradients for ONSA (red dots) and ONS1 (black dots). The VLBI observations include the days 126–140 (6–20 May).
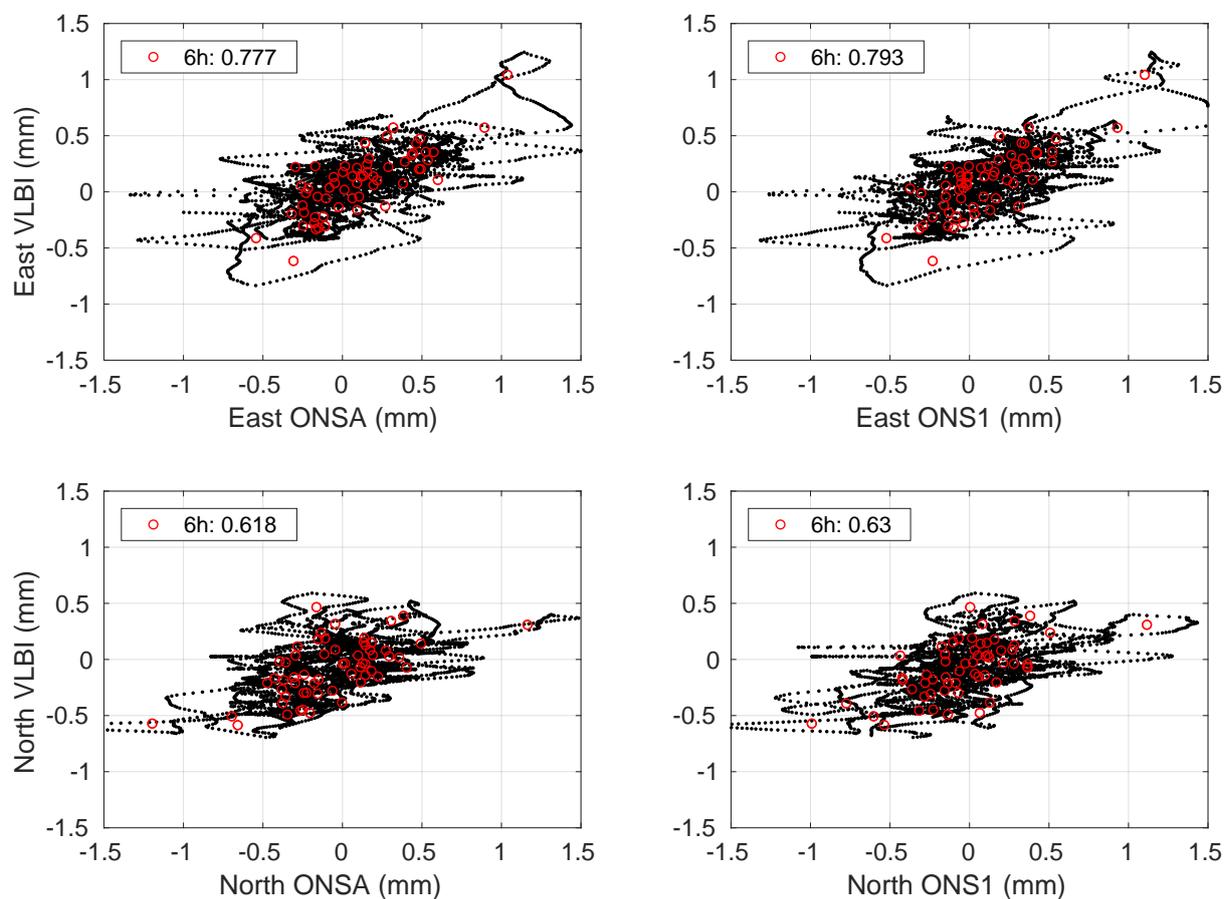
Figure 15. Correlation plots of the total estimated VLBI gradients vs the total gradients from the two GPS sites, ONSA and ONS1 during the CONT14 campaign. The red circles are at the epochs of the VLBI estimates, every 6 h, and the black dots are linearly interpolated VLBI results with a temporal resolution of 5 min in order to match the GPS data. The correlation coefficients presented in the graphs are calculated using mean values for the period of ± 3 h around the time epochs of the VLBI values (6h:).

6   Conclusions

We have shown that estimated linear horizontal gradients from GPS data in Sweden can be understood based on meteorological phenomena. Averaging gradients in the east and the north direction over one month gives correlation coefficients of up to 0.9 when compared to gradients calculated from meteorological analyses of the ECMWF. Monthly averages of the gradients are
5   dominated by the hydrostatic component.

When studying gradients averaged over shorter time scales, e.g. 15 min, we find the wet component of the gradients to cause most of the variability. Correlation coefficients between wet gradients from GPS can for specific months reach up to 0.8 when compared to simultaneously estimated wet gradients from the WVR. Based on the four years of results we note a strong seasonal dependence, from 0.3 during months with smaller gradients to 0.8 during months with larger gradients, typically
10   during the warmer, and more humid, part of the year.

In general we also note slightly higher correlation coefficients for the GPS derived gradients in the east compared to the north direction. We interpret this difference to be caused by an inhomogeneous spatial sampling on the sky, which is important when we assume that the model describing linear horizontal gradients has deficiencies. The different sampling on the sky is an important issue for any comparison between different techniques.

15   No significant long-term trends were detected for the horizontal gradients. If small gradients trends are detected in the future we recommend to critically assess if they could be caused by station problems or confirmed by a nearby (or even collocated) site.

Author contributions.   Gunnar Elgered coordinated and wrote the major part of the manuscript and together with Tong Ning planned the different GNSS data analyses during the COST Action ES1206. Tong Ning performed the GNSS data analyses, resulting in the estimated
20   horisontal gradients. Peter Forkman and Rüdiger Haas carried out the same task for WVR and VLBI data, respectively. All authors contributed in the writing process, in particular to the sections presenting the results produced by each author and approved the entire manuscript before the submission.

Competing interests.   The authors declare that they have no conflict of interest.

Acknowledgements.   The map in Figure 2 was produced using the Generic Mapping Tools (Wessel and Smith, 1998).

References

Bar-Sever, Y.-E., Kroger, P. M., and Börjesson, J. A.: Estimating horizontal gradients of tropospheric path delay with a single GPS receiver, J. Geophys. Res., 103(B3), 5019–5035, 1998.

Bertiger, W., Desai, S.D., Haines, B., Harvey, N., Moore, A.W., Owen, S., and Weiss, J.P.: Single receiver phase ambiguity resolution with
5   GPS data, J. Geod., 84:327–337, doi:10.1007/s00190-010-0371-9, 2010.

Boehm, J., Werl, B. and Schuh, H.: Troposphere mapping functions for GPS and very long baseline interferometry from European Centre for Medium-Range Weather Forecasts operational analysis data, J. Geophys. Res., 111, B02406, doi:10.1029/2005JB003629, 2006.

Boehm, J. and Schuh, H.: Troposphere gradients from the ECMWF in VLBI analysis, J. Geod., 81:403–408, doi: 10.1007/s00190-007-0144-2, 2007.

10 Brown, R. A.: A secondary flow model for the planetary boundary layer, J. Atmos. Sci., 27, 742–757, 1970.

Bruyninx, C., Habrich, H., Söhne, W., Kenyeres, A., Stangl, G., and Völksen, C.: Enhancement of the EUREF Permanent Network Services and Products, Geodesy for Planet Earth, IAG Symposia Series, 136, 27–35, doi:10.1007/978-3-642-20338-1_4, 2012.

Davis, J. L., Elgered, G., Niell, A. E., and Kuehn, C. E.: Ground-based measurement of gradients in the "wet" radio refractivity of air, Radio Sci., 28(6), 1,003–1,018, doi:10.1029/93RS01917, 1993.

15 Douša J., Václavovic P., Eliaš, M.: Tropospheric products of the second European GNSS reprocessing (1996–2014), Atmos. Meas. Tech., 10:1–19, doi:10.5194/amt-10-1-2017, 2017.

Gradinarsky, L. P., Haas, R., Elgered, G., and Johansson, J. M.: Wet path delay and delay gradients inferred from microwave radiometer, GPS and VLBI observations, Earth Planets Space, 52(10), 695–698, 2000.

Hewson, E. W. and Longley, R. W.: Meteorology: Theoretical and Applied, New York, John Wiley & Sons, 1944

20 Li, X., Zus, F., Lu, C., Ning, T., Dick, G., Ge, M., Wickert, J., and Schuh, H.: Retrieving high-resolution tropospheric gradients from multiconstellation GNSS observations, Geophys. Res. Lett., 42(10), 4173–4181, 2015.

Lu, C., Li, X., Li, Z., Heinkelmann, R., Nilsson, T., Dick, G., Ge, M., and Schuh, H.: GNSS tropospheric gradients with high temporal resolution and their effect on precise positioning, J. Geophys. Res. Atmos., 121, 912–930, doi:10.1002/2015JD024255, 2016.

Lyard F., Lefevre, F., Letellier, T., and Francis, O.: Modelling the global ocean tides: Modern insights from FES2004, Ocean Dyn., 56, 394,
25 doi:10.1007/s10236-006-0086-x, 2006.

Ma C., Sauber J. M., Bell L. J., Clark T. A., Gordon D., Himwich W. E., and Ryan J. W.: Measurement of horizontal motions in Alaska using very long baseline interferometry, J. Geophys. Res., 95, 21991–2011, 1990.

Matteo, N. A., and Morton, Y. T.: Ionosphere geomagnetic field: Comparison of IGRF model prediction and satellite measurements 1991-2010, Radio Sci., 46, RS4003, doi:10.1029/2010RS004529, 2011.

30 Meindl, M., Schaer, S., Hugentobler, U., and Beutler, G.: Tropospheric Gradient Estimation at CODE: Results from Global Solutions, J. Meteorol. Soc. Japan, 82, 331–338, doi:10.2151/jmsj.2004.331, 2004.

Munn, R. E.: Descriptive Micrometeorology, Academic Press, New York, 1966.

Niell, A. E.: Global mapping functions for the atmosphere delay at radio wavelengths, J. Geophys. Res., 101(B2), 3227–3246, doi:10.1029/95JB03048, 1996.

35 Ning, T., Elgered, G., Willén, U., and Johansson, J.M.: Evaluation of the atmospheric water vapor content in a regional climate model using ground-based GPS measurements, J. Geophys. Res., 118, 1–11, doi: 10.1029/2012JD018053, 2013.

Nothnagel, A., Artz, T., Behrend, D. , and Malkin, Z.: International VLBI Service for Geodesy and Astrometry Delivering high-quality products and embarking on observations of the next generation J. Geod., 91, 711–721, doi: 10.1007/s00190-016-0950-5, 2017.

Schmid, R., Steigenberger, P., Gendt, G., Ge, M., Rothacher, M.: Generation of a consistent absolute phase center correction model for GPS receiver and satellite antennas, J. Geod., 81, 781–798, doi:10.1007/s00190-007-0148-y, 2007.

5 Teke, K., Nilsson, T., Böhm, J., Hobiger, T., Steigenberger, P., Garcia-Espada, S., Haas, R., and Willis, P.: Troposphere delays from space geodetic techniques, water vapor radiometers, and numerical weather models over a series of continuous VLBI campaigns, J. Geod., 87, 981–1001, doi 10.1007/s00190-013-0662-z, 2013.

Webb, F. H. & Zumberge, J. F.: An Introduction to the GIPSY/OASIS-II, JPL Publ., D-11088, Jet Propulsion Laboratory, Pasadena, California, 1993.

10 Wessel, P. and Smith, W. H. F.: New, improved version of generic mapping tools released, EOS Trans. Amer. Geophys. U., 79(47), 579, doi:10.1029/98EO00426, 1998.

Zumberge, J. F., Heflin, M. B., Jefferson, D. C., Watkins, M. M., and Webb, F. H.: Precise point positioning for the efficient and robust analysis of GPS data from large networks, J. Geophys. Res., 102, 5005–5017, 1997.